

An Integrated Computational Approach to the Phenomenon of Potent and Selective Inhibition of Aurora Kinases B and C by a Series of 7-Substituted Indirubins

Vassilios Myrianthopoulos,[†] Prokopios Magiatis,[†] Yoan Ferandin,[‡] Alexios-Leandros Skaltsounis,[†] Laurent Meijer,[‡] and Emmanuel Mikros^{*†}

School of Pharmacy, University of Athens, Panepistimiopolis Zografou, GR-15771, Athens, Greece, and Cell Cycle Group, Station Biologique, Centre National de la Recherche Scientifique, B.P. 74, 29682 Roscoff Cedex, Bretagne, France

Received January 19, 2007

A variation of the bromine substitution from 6- to 7-position converts the glycogen synthase kinase-3 α/β - (GSK-3- α/β) selective inhibitor 6-bromoindirubin-3'-oxime (6BIO) to a potent inhibitor of Aurora B and C kinases. The novel indirubin analogue 7-bromoindirubin-3'-oxime (7BIO) demonstrated unexpected selectivity against these two kinases since the homologous kinase Aurora A was poorly inhibited. A hypothesis regarding the 7BIO selectivity profile was stated and validated by docking, molecular dynamics, and free energy perturbation calculations. The residue (Thr217^{AurA}, Glu161^{AurB}, Glu127^{AurC}) located in the active site was identified as a major contributor to the enhanced affinity of 7BIO for Aurora B and C versus Aurora A. Furthermore, the docking events of 7BIO and several of its analogues were approached by quantitative models based on semiempirical scoring functions. In the course of model construction and optimization, a number of important factors influencing the quality of each model like the application of force constraints or the sampling method were determined. Among these factors, the presence and treatment of structurally important water molecules had a pronounced impact on the quality of each model. The final model was validated by use of free energy perturbation calculations.

Introduction

The large family of protein kinases (518 members in the human kinome) includes some of the most promising targets aimed by the search for chemotherapeutic drugs.^{1,2} A large amount of evidence supports the fact that various kinases are deregulated in cancer cells, in neurodegenerative diseases, and in inflammation.^{3–8} Inhibition of the malfunctioning tyrosine or serine–threonine kinases has been proposed as a valid approach to the treatment of numerous diseases. Several drugs potently inhibiting such receptor tyrosine kinases have reached clinical trials, and two compounds, imatinib (Gleevec) and gefitinib (Iressa), are already in clinical use as chemotherapeutic drugs.⁹ However, side effects arise from the simultaneous inhibition of properly regulated kinases of the organism. The high degree of similarity of the ATP binding site among members of the kinase family is one of the reasons many known inhibitors show limited selectivity.¹⁰ As a result and without neglecting the possible advantages of multitarget drugs, selectivity is one of the factors determining the value of a kinase inhibitor either as a therapeutic agent or as a tool for the study of biochemical events.

The molecular scaffold of indirubin provides an excellent basis for the development of highly potent protein kinase inhibitors. The discovery of indirubin as a potent inhibitor of cyclin-dependent kinases (CDKs)⁶ and the crystallographic determination of two of its derivatives, indirubin-3'-oxime and

indirubin-5-sulfonate, complexed with CDK2 has assisted the design and synthesis of a series of 5-substituted analogues, with the most active derivatives being the 5-iodo-3'-oxime and the 5-sulfonate-3'-oxime analogues.¹¹ Indirubin potency, as revealed by crystallographic studies of various CDK2–inhibitor complexes, is a result of the molecule's pharmacophore perfect topology, which allows an optimal interaction mode with the binding site through the formation of three hydrogen bonds.¹² The pharmacophore consists of the lactam nitrogen, the lactam oxygen, and the heterocyclic nitrogen of the molecule, which interact with the receptor backbone and anchor the inhibitor molecule in the active site in the usually observed adenine-type mode. The isolation from gastropod mollusks of a novel natural indirubin analogue bearing a 6-bromo substitution and its selectivity toward GSK-3 guided the design and synthesis of 6-substituted and 5,6-disubstituted analogues.^{13,14} Modeling studies suggested that substitution in positions 5 and 6 would optimize the binding affinity and selectivity for GSK-3 β .¹⁴ At the same time, modeling combined with the crystallographic determination of the complex of 6-bromoindirubin 3'-oxime (6BIO) bound to GSK-3 β shed some light on the structural basis for the compounds' selectivity. In GSK-3 β the bromine atom at position 6 occupies a highly buried hydrophobic pocket of the receptor active site, the entrance to which is controlled by the side chain of the "gatekeeper" residue Leu132. 6BIO inhibits GSK-3 β more potently than CDK5/p25 and CDK1/cyclin B, by 1 and 2 orders of magnitude respectively. The corresponding residue of leucine132^{GSK-3 β} is a phenylalanine in the CDKs. The steric clash between the bromine atom and the phenylalanine side chain has been described as the major cause of the decreased binding affinity of 6BIO, and 6-substituted analogues, for CDKs. This example of selective kinase inhibiting indirubins illustrates another advantageous characteristic of these bisindole compounds, namely, the possibility of designing and synthesizing analogues demonstrating high selectivity toward specific kinase targets. The core of the indirubin scaffold indeed provides

* To whom correspondence should be addressed: tel 30 2107274813; fax 30 2107274747; e-mail mikros@pharm.uoa.gr.

[†] University of Athens.

[‡] CNRS.

⁶ Abbreviations: CDK, cyclin-dependent kinases; GSK-3 β , glycogen synthase kinase-3 β ; 6BIO, 6-bromoindirubin-3'-oxime; 7BIO, 7-bromoindirubin-3'-oxime; 7CLIO, 7-chloroindirubin-3'-oxime; 7IIO, 7-iodoindirubin-3'-oxime; 7FIO, 7-fluoroindirubin-3'-oxime; 7BIMe, 7-bromoindirubin-3'-methoxime; 7BIAc, 7-bromoindirubin-3'-acetoxime; 7IIMe, 7-iodoindirubin-3'-methoxime; 7IIAc, 7-iodoindirubin-3'-acetoxime; DTT, dithiothreitol; BSA, bovine serum albumin; FEP, free energy perturbation.

numerous sites where chemical groups can be introduced to increase selectivity without affecting potency.

According to the data obtained by modeling and by crystallography, a 7-substitution, especially a bulky one, was expected to diminish potency since it would collide with the receptor backbone and cause unfavorable contacts or distort the geometry of the hydrogen bonds responsible for binding. Yet, in order to perform a complete quantitative structure–activity relationship study of indirubin analogues, 7-bromoindirubin-3'-oxime (7BIO) was prepared.¹⁵ The initial hypothesis was confirmed by tests of 7BIO on GSK-3 β , CDK1 and CDK5, where 7BIO was essentially inactive.¹⁶ The same was true for Aurora A kinase, which was inhibited with an IC₅₀ of 100 μ M. However, an unexpected result was obtained when 7BIO was tested against Aurora B and C. It inhibited these two kinases with IC₅₀ values of 4.6 μ M and 0.7 μ M, respectively. Aurora A, B, and C are closely related homologues that share a high degree of sequence similarity, especially among the active-site residues. As a result, 7BIO seemed to demonstrate a novel kind of selectivity profile.

The serine–threonine kinases Aurora A and B and the least studied Aurora C are regulatory proteins that play a key role in the mitotic events of cellular division.^{17–19} Aurora A and B have distinct roles in mitosis. While Aurora A mainly regulates mitotic spindle assembly and centrosome maturation, Aurora B is involved in chromosome segregation and cytokinesis.²⁰ Aurora C is, like Aurora B, a chromosomal passenger protein cooperating with Aurora B in the regulation of mitotic chromosome segregation and cytokinesis, but its exact function and regulation are not yet fully understood. As with other kinases that are essential for cell division, improper regulation or overexpression of the Aurora kinases can lead to genetic instability and tumorigenesis. Evidence exist that the three Aurora kinases are frequently overexpressed in many human tumors.²¹ Aurora overexpression is observed in colorectal, breast, pancreatic, and other cancers.^{22–25} Moreover, Aurora A overexpression causes increased degradation of the natural tumor suppressor p53.²⁶ Aurora B is also overexpressed in cancer cells and is suggested to induce tumor metastasis.^{27,28} Although overexpression is not definitely linked with carcinogenesis, and various issues remain to be addressed about the mechanisms implicating Aurora activity with tumorigenesis, they appear as promising targets for the development of chemotherapeutic drugs. Indeed, several selective Aurora kinase inhibitors have emerged in the literature, either as drug candidates or as biochemical tools. Examples include AstraZeneca AZD1152, Vertex VX-680 that has entered in clinical trials, Hesperadin, and ZM447439.^{29,30}

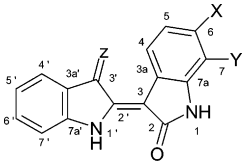
To provide a rationale for this exceptional selectivity profile of 7BIO, our assumption was that the experimentally observed divergence in the inhibitory potential of 7BIO toward the three homologous kinases is caused by differences in the amino acid sequence and more specifically in the binding pocket. In this work we present the comparison of the three Aurora kinase structures; Aurora B and C were constructed by homology to the Aurora A crystal structure. Interestingly, a single residue in the ATP binding pocket appeared to be sufficient to rationalize the activity differences between Aurora A, B, and C. In order to gain insight in the binding process of 7BIO and various active or inactive indirubin analogues, theoretical calculations were undertaken. The correlation of the experimentally determined binding affinities with the calculated binding energies led to the construction of a theoretical model simulating the protein–ligand interactions. In the course of model optimization, valuable

information concerning issues at the methodological level were obtained. By elucidating the impact of various methodological factors, with emphasis on force constraints, binding microenvironment topology, and structural water molecules, the correlation of experimental versus calculated binding affinities was optimized. Finally, the utilization of two more accurate simulation methods, namely, molecular dynamics and free energy perturbation, further verified our hypothesis.

Results and Discussion

Chemistry. Indirubins substituted on position 7 with F, Cl, Br, and I, as well as their 3' oxime, methoxime, and acetoxime analogues plus unsubstituted indirubins, were prepared as previously described¹⁵ and are presented in Table 1 along with their biological activities in Aurora kinases A, B, and C. In contrast with the unsubstituted and 6-substituted analogues **1–4** that inhibit equipotently the three kinases, 7-substituted oximes **5, 9, and 17**, carrying a halogen bulkier than fluorine, demonstrate selective inhibition of Aurora B and C. Methylation and acetylation of the oximes diminishes activity more than 2 orders of magnitude compared to the nonsubstituted derivatives, with the exception of **7**, where a \sim 10-fold decrease was observed.

Homology Model Building. The crystal structures of the human Aurora kinases B and C are not yet determined. On the contrary, several crystallographic studies of human Aurora A are available, both of the active and the inactive states.^{31,32} Homology models of Aurora B and C were built by using the structure of the active Aurora A bound to ATP (1MQ4) as a template. In this structure, the activation loop adopts an extended conformation allowing access to the ATP binding pocket. The sequence alignment of the three receptors that share a high degree of identity, over 68%, is depicted in Figure 1. Forty homology models were built and refined by use of the loop optimization routine and a slow simulated annealing protocol as implemented in MODELLER software.³³ The best model was selected by a consensus of the program objective function and stereochemical quality scores (0% residues in disallowed regions of Ramachandran plot, overall *G*-score >0.01) calculated by PROCHECK.³⁴ The quality and stability of the two final homology models were tested by a stochastic dynamics (SD) simulation of 100 ps equilibration and 400 ps run. The root-mean-square deviation of the C α atoms from starting coordinates was measured throughout the simulation (Scheme 1). The good stability of the models was expected since Aurora B and C share a high degree of similarity with Aurora A. The greater SD deviations appeared in the flexible parts of the receptor like the glycine loop but also in the activation loop and in the N-terminus. Sequence alignment and three-dimensional models showed that the residue which is, in many cases, responsible for selectivity between kinases, the so-called “gatekeeper residue”, is identical in the three Aurora sequences and it is a leucine (Leu210^{AurA}, Leu156^{AurB}, and Leu120^{AurC}). More importantly the sequence alignment showed that there are only four residues located in the vicinity of the ATP binding site that are not identical in the three kinases (Figure 2). In particular leucine 215 of Aurora A is replaced by an arginine in Aurora B and C (Arg159^{AurB}, Arg125^{AurC}), threonine 217 of Aurora A is replaced by a glutamate in Aurora B and C (Glu161^{AurB}, Glu127^{AurC}), valine 218 of Aurora A is replaced by a leucine in Aurora B and C (Leu162^{AurB}, Leu128^{AurC}) and arginine 220 of Aurora A is replaced by a lysine in Aurora B and C (Lys164^{AurB}, Lys130^{AurC}). The least important seems to be the replacement of valine by leucine, given that both residues are apolar and their side chains point away from the pocket. The

Table 1. IC₅₀ Values of the Synthesized Analogues^a


compound	X	Y	Z	IC ₅₀ (μM)		
				Aurora A	Aurora B	Aurora C
1	H	H	NOH	4.0	2.3	0.3
2	H	H	NOCH ₃	4.3	3.0	0.4
3	H	H	NOAc	2.3	2.1	0.7
4	Br	H	NOH	0.6	0.9	0.2
5	H	Br	NOH	100.0	4.6	0.7
6	H	Br	NOCH ₃	> 100.0	> 100.0	> 100.0
7	H	Br	NOAc	> 100.0	20.0	4.5
8	H	Br	O	> 100.0	> 100.0	> 100.0
9	H	Cl	NOH	> 100.0	8.0	0.9
10	H	Cl	NOCH ₃	> 100.0	> 100.0	> 100.0
11	H	Cl	NOAc	> 100.0	> 100.0	> 100.0
12	H	Cl	O	> 100.0	> 100.0	> 100.0
13	H	F	NOH	2.0	7.0	1.0
14	H	F	NOCH ₃	> 100.0	> 100.0	> 100.0
15	H	F	NOAc	20.0	8.0	1.0
16	H	F	O	> 100.0	> 100.0	> 100.0
17	H	I	NOH	> 100.0	10.0	0.6
18	H	I	NOCH ₃	> 100.0	> 100.0	> 100.0
19	H	I	NOAc	> 100.0	> 100.0	28
20	H	I	O	> 100.0	> 100.0	> 100.0

^a A series of indirubin analogues were tested at various concentrations in three kinase assays, as described in the Materials and Methods section. IC₅₀ values were calculated from the dose–response curves and are reported as micromolar concentrations.

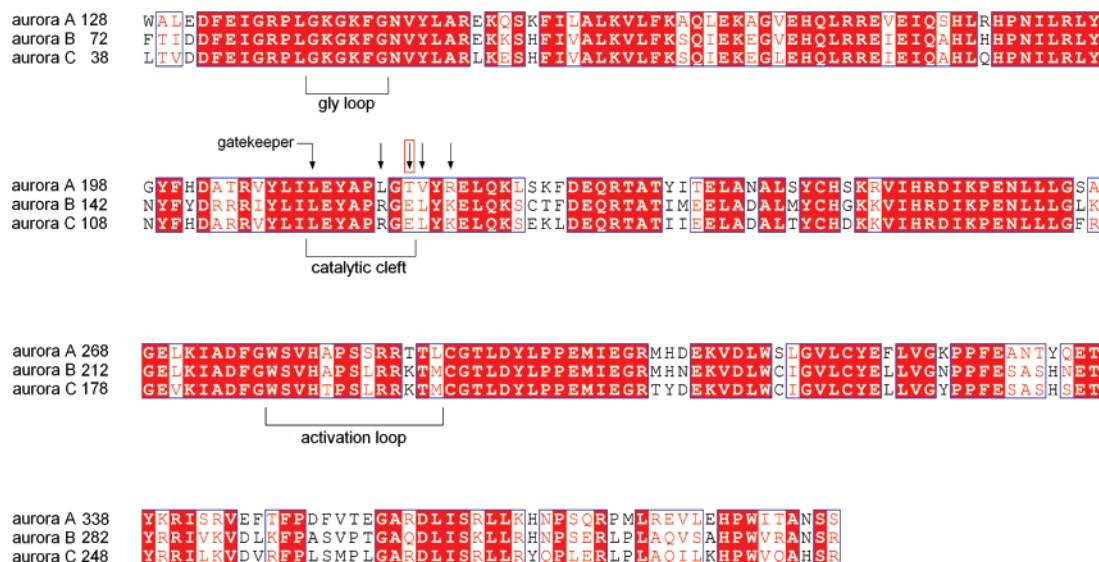


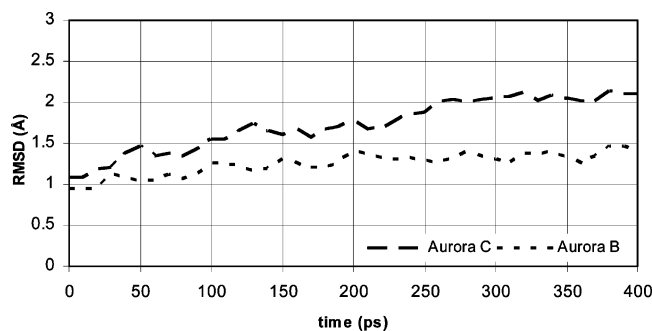
Figure 1. Sequence alignment of the three human Aurora protein kinases. Identical residues are enclosed in red boxes. Similar residues are noted as red characters in blue boxes. The five arrows indicate the “gatekeeper” as well as the four residues of the active site that are not identical in the three kinases. The critical glutamate is denoted by the red boxed arrow.

replacement of leucine by arginine seems to be of mediocre significance, as the two residue side chains are directed toward the solvent and away from the catalytic pocket. The same is true for the replacement of arginine by lysine, as both residues share the same basic character and their side chains point to the solvent. On the contrary, the replacement of threonine by glutamate should be considered of great importance. In this case a polar residue is replaced by an acidic one having a longer and more flexible side chain. This residue is located near the edge of the catalytic pocket, in a subsite referred to as the ribose binding region. It is a hydrophilic part of the binding site, where interactions between the receptor and the sugar moiety of the

natural substrate are formed, as demonstrated in crystal structures like adenosine complexed with cAMP-dependent kinase (1FMO) or ATP complexed with CDK2 (1HCK). Moreover, crystallography studies revealed that residues located in the ribose binding site interact with inhibitors, either directly (olomoucine bound to CDK2, 1W0X; roscovitine bound to CDK5/p25, 1UNL) or through water molecules (indirubin-3'-oxime bound to CDK5/p25, 1UNH; 6BIO bound to GSK-3β, 1UV5) enhancing ligand affinity.

We have hypothesized that this glutamate residue located on the edge of the binding pocket (Glu161^{AurB}, Glu127^{AurC}) is the main contributor to the selectivity profile demonstrated by the

Scheme 1. Root-Mean-Square Deviation of the Aurora B and C Homology Models C $_{\alpha}$ Trace from Starting Coordinates as a Function of Stochastic Dynamics Simulation Time



inhibitory indirubin 7BIO. A comparison of the IC₅₀ values of 7BIO and 6BIO (Table 1) shows that 7BIO is 3 orders of magnitude less potent in the case of Aurora A ($AurAIC_{50}$ changes from 0.6 μ M to 100 μ M). However, in Aurora B and C the affinity of 7BIO compared to that of 6BIO is decreased only by a 5-fold factor ($AurBIC_{50}$ changes from 0.9 μ M to 4.6 μ M) and a 3.5-fold factor ($AurCIC_{50}$ changes from 0.2 μ M to 0.7 μ M), respectively. The side-chain carboxylate of glutamate was assumed to form strong stabilizing electrostatic interactions with the oxime moiety of the ligand. The corresponding residue of Aurora A, threonine 217, carrying a shorter, less polar, and nonionizable side chain, could not possibly offer equally strong interactions, thus explaining the selective inhibition of Aurora B and C by 7BIO. In order to confirm this hypothesis, docking calculations were undertaken. Energy calculations were expected to verify the aforementioned differences in biological results and provide insight in the binding events of indirubin analogues in the Aurora kinase targets.

Docking Calculations. Our main effort was to correlate structural differences in the microscopic environment of each kinase active site with macroscopic biological results derived from binding affinity calculations. In order to perform reproducible and valid docking calculations as well as to get a computational reproduction of experimental binding affinities of indirubin analogues in the Aurora kinases, several methodological issues were considered. The parameters that had to be well tuned were the sampling method, the topology of the binding site microenvironment along with harmonic constraints applied on critical residues, and the manipulation of structurally important water molecules.

The interaction mode of the indirubin pharmacophore is very similar among all crystal structures of indirubin analogues bound to kinase receptors (indirubin–CDK5/p25, 1UNH; 5-bromoindirubin–CDK2, 2BHE; indirubin-5-sulfonate–CDK2/cycA, 1E9H; 6-bromoindirubin-3'-oxime–GSK-3 β , 1UV5) and consists mainly of three hydrogen bonds formed between the receptor and the heteroatoms of the planar aromatic system of the inhibitor. Docking trials performed with Monte Carlo searches resulted in a global minimum conformation where the indirubin molecule was stabilized only through hydrophobic interactions without forming any hydrogen bonds with the receptor. The strength of these stacking interactions had caused the molecule being originally flat to adopt a slightly curved conformation, leading it to bury itself in an irrational mode in the binding pocket (data not shown). Such docking errors could be attributed to a deficiency of the force field that leads to an overestimation of the hydrophobic versus the electrostatic interactions where hydrogen bonding is implicitly included. The serious deviation from the expected crystallography-based low-energy structure was the reason that prompted us to protect the

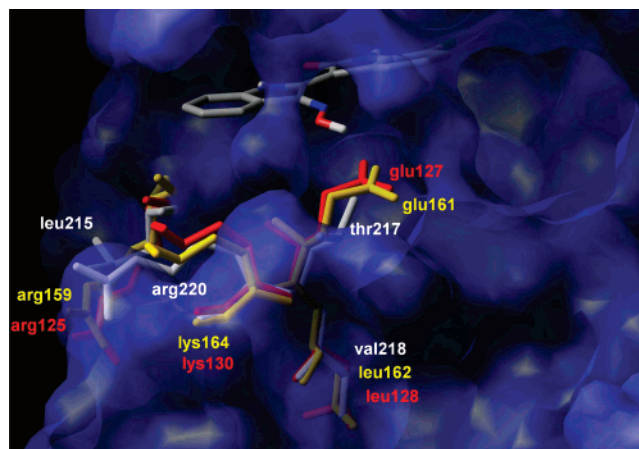


Figure 2. Location of the four residues of the active site that are not identical in the three Aurora kinases. White refers to Aurora A, yellow to Aurora B, and red to Aurora C. The most significant difference that discriminates Aurora A from Aurora B and C is the replacement of Thr217^{AurA} by a glutamate (Glu161^{AurB}, Glu127^{AurC}). This particular residue interacts with the bound ligand while the other three amino acids are located away from the ATP-binding pocket entrance.

formation of the three key hydrogen bonds by harmonic force constraints, simulating the knowledge-based approach used for optimizing scoring functions. We have applied a stepwise minimization scheme focused on these key bonds. In the first step, 6BIO was docked in the ATP binding pocket and an energy minimization was performed with distance and donor/acceptor angle constraints (three distances and six angles restrained) on the three key hydrogen bonds. Their geometry was restrained to the crystallographically determined values as they appear in the structure of 6BIO bound to GSK-3 β . In a second step, an unconstrained minimization followed. All other ligands were superimposed on the previously docked ligand. In this way the molecules were trapped in the energy minimum where the three hydrogen bonds occur. An additional set of constraints applied on the three residues participating with their backbone atoms in the hydrogen bonds was utilized, aiming at a further stabilization of this key interaction pattern. The restrained residues were Glu211^{AurA}, Tyr212^{AurA}, and Ala213^{AurA}; Glu155^{AurB}, Tyr156^{AurB}, and Ala157^{AurB}; and Glu121^{AurC}, Tyr122^{AurC}, and Ala123^{AurC}, all belonging to the hinge region between the N and the C-termini of the protein. The side chains of these residues are located away from the pocket, they do not directly interact with the ligand, and their reduced mobility would not influence the results. In the course of docking and subsequent interaction energy calculation of the various ligand–protein complexes, we have utilized minimization as a sampling method. Although in many cases of computational evaluation of free energy of binding more sophisticated methods like molecular dynamics or Monte Carlo searches have been used, it has been argued that a simple minimization scheme is adequate and a much more demanding sampling method does not really improve results.^{36–38}

A second set of force constraints concerned the side chains of Arg137^{AurA} and Arg220^{AurA}, Arg81^{AurB}, and Arg47^{AurC}. In the course of preliminary docking trials, the arginine side chain that forms the left-side “wall” of the pocket demonstrated an ambiguous attitude that was considered as an artifact. This arginine belongs either in the N-terminal or in the C-terminal domain of the protein but its side chain projects toward the hinge region. A study of crystal structures of ligands complexed with kinases bearing an arginine at this position revealed that in the presence of an inhibitor the guanidine moiety of arginine usually

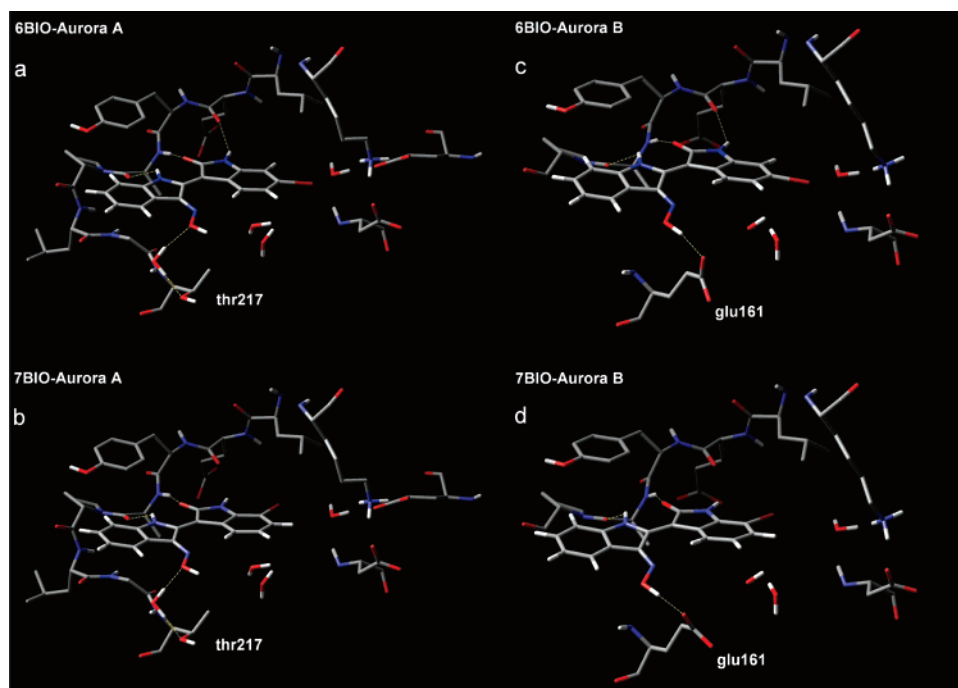


Figure 3. (a) 6BIO bound to Aurora A forming three direct hydrogen bonds. (b) 7BIO bound to Aurora A, where only two direct hydrogen bonds are formed. The hydrogen bond between the lactam nitrogen at position 1 of indirubin and the receptor is not formed because of the steric clash between the 7-Br and the kinase backbone. (c) 6BIO bound to Aurora B, forming the same pattern of hydrogen bonds observed in the 6BIO–Aurora A complex. (d) When 7BIO is bound to Aurora B (and C), the hydrogen bond between the nitrogen at position 1 of indirubin and the receptor is not formed, as in the case of 7BIO–Aurora A. However, a novel direct hydrogen bond is formed between the oxime and the side chain of a critical glutamate present in Aurora B (Glu161^{AurB}) and C (Glu127^{AurC}). As a result, 7BIO retains its potency toward Aurora B and C.

forms either a cation– π or π – π interaction with the aromatic system of the inhibitor (6BIO bound to GSK-3 β , 1UV5; alsterpaullone bound to GSK-3 β , 1Q3W; AR-A014418 bound to GSK-3 β , 1Q5K) or it is oriented toward the solvent. In that case it forms either no interactions with the ligand (ADP bound to Aurora A/TPX2, 1OL5) or indirect interactions mediated by water molecules (ADP bound to Aurora A, 1MQ4). Docking trials showed that the guanidine moiety of arginine was attracted by the aromatic system of indirubin. This resulted in structures where the guanidine tended to intercalate between the aromatic system of the ligand and the hydrophobic pocket of the kinase, orienting itself at an angle to the ligand plane. We considered that this was possibly a case of overestimation of hydrophobic interactions by the force field, which would lead to a wrong estimation of the interaction energy. It was decided to restrain this residue side chain in its starting coordinates. Subsequent comparison between models constructed with and without constraints on this residue would validate our approach. With the exception of the aforementioned sets of constraints, our calculations have been performed in a flexible kinase. All atoms belonging to residues 6 Å around the ligand were free to move and the remaining residues were not extracted but considered as frozen. In most cases of computational reproduction of binding affinities, a rigid receptor is used and similar constraints are not required; nevertheless, studies where a rigid receptor approach is combined with hydrogen bond constraints have been described.³⁹

The molecules placed in the active site as described were fully energy-minimized. Comparison of the resulting structures obtained for 6BIO and 7BIO have clearly shown that when the substitution pattern is converted from 6-halo (Figure 3a,c) to 7-halo (Figure 3b,d), a steric clash occurs between the atom positioned in place 7—in our case a bromine—and the kinase. This clash forces the inhibitor to adopt a slightly different

orientation in the pocket in order to relieve the unfavorable contact. This new orientation, however, has an impact on the three hydrogen bonds formed between the pharmacophore and the receptor backbone that comprise the key interactions of the complex. Their geometry changes and this perturbation has a negative impact on the strength of each bond. The most distorted bond is the one formed between the proton of the lactam nitrogen at position 1 of indirubin and the backbone carbonyl of glutamate (Glu211^{AurA}, Glu155^{AurB}, Glu121^{AurC}). The decrease of the bond strength is reflected in the loss of 7BIO binding affinity for Aurora A (Table 1). In Aurora B and C, however, this enthalpic loss is efficiently equalized by a novel direct hydrogen bond formed between the oxime hydrogen of the inhibitor and the side-chain carboxylate of the critical glutamate (Glu161^{AurB}, Glu127^{AurC}) located at the ribose site. The equilibration of the key hydrogen bond loss by this novel interaction in Aurora B and C is manifested in the calculated interaction energies of the ligand–receptor complexes. The difference between the electrostatic terms for the complexes 6BIO–Aurora A and 7BIO–Aurora A is +5.81 kJ/mol, representing the loss from the distorted hydrogen-bond formation. This difference is diminished in Aurora B to –0.24 kJ/mol and in Aurora C to +0.6 kJ/mol due to the novel stabilizing interaction offered by the glutamate side chain (values obtained from model 3; see following paragraph).

The results of this qualitative approach in the binding events were encouraging, but they were not sufficient to validate our selectivity hypothesis. Construction of a quantitative model correlating experimental and calculated binding affinities of a set of six different indirubin analogues (6BIO, 7BIO, 7FIO, 7CLIO, 7BIME, and 7BIAC) was selected as the validation method of choice.

Model Construction. We have followed a semiempirical scoring function for approximating the calculated binding

affinities. The free energy of binding is calculated by

$$\Delta G_{\text{calc}} = \alpha E_{\text{electrostatic}} + \beta E_{\text{vanderWaals}} + \gamma \quad (1)$$

as the weighted sum of two individual energy terms concerning the interaction between the protein and the ligand, the electrostatic and the hydrophobic or van der Waals term, plus an empirical coefficient. The weighting coefficients come from a regression analysis, where the computed interaction energies ΔG_{calc} are fitted to the experimental free energies of binding ΔG_{exp} . Correlation of the calculated versus experimental binding affinities and the resulting coefficient of determination r^2 would be used as a measure of the model success. Calculated free energies of binding from the models described below are summarized in Table 2 along with the experimental values derived from IC₅₀. Individual interaction energy terms, electrostatic and vdW, obtained from each model along with weighting coefficients α , β , and γ are also provided as Supporting Information (Tables S1 and S2).

The environment in the vicinity of each of the three Aurora kinases active sites constitutes a highly similar structural landscape, as was expected from homology. Thus, the scoring function was reasonably assumed to be common for the three enzymes. Deviations or small conformational variations in distant residues were expected to have only a modest influence on the correlation quality. On the contrary, special attention was paid to residues located in critical positions around the ATP-binding pocket so that they would have an identical side-chain conformation in all starting structures.

The final issue that was considered regarding model preparation was the presence of structurally important water molecules. At a first step (primary model), two crystallographic water molecules from the template structure (1MQ4) named water molecules A_w and B_w were retained in the calculations (Figure 4). Water A_w (PDB atom 2090) is buried deep in the ATP-binding pocket, between the hydrophobic site of the pocket and the catalytic Lys-Asp-Glu group. A water molecule is positioned in a conserved mode in the ATP-CDK2/cyclin A (1FIN) and 6BIO-GSK-3 β (1UV5) structures as well. In these structures ligand binding does not lead to the displacement of this water molecule. The second water molecule (water B_w, PDB atom 2089) is located 3.6 Å from the side-chain hydroxyl group of Thr217. As observed in other kinase crystal structures having a threonine as a corresponding residue in this position like in the GSK-3 β -6BIO complex, the ligand interacts indirectly with the hydroxyl group of threonine (Thr138) and this interaction is mediated by two water molecules.¹⁴ This interaction is proposed to account for the improved affinity of oxime analogues compared to non-oxime indirubins. This is the case in the Aurora A-ADP structure also, where two water molecules bridge the corresponding threonine (Thr217) hydroxyl with the purine nitrogen of ADP (water molecules 2089 and 3036). However, only one of them was kept (named B_w, PDB 2089). The other was eliminated due to a possible overlap with the larger indirubin molecule compared to that of adenine of ADP. The difference between indirubin interacting with Thr138^{GSK-3 β} through two water molecules and indirubin interacting with Thr217^{AurA} through one is caused by the presence of an additional glycine (Gly216) in the Aurora A sequence. This additional glycine brings the threonine residue closer to the boundary of the pocket where the oxime moiety is expected to be located. Water B_w was retained only in the Aurora A system, since in Aurora B and C it is expected to be displaced by the side chain of the glutamate (Glu161^{AurB}, Glu127^{AurC}) corresponding to Thr217^{AurA}.

Table 2. Calculated Free Energies of Binding from Various Models Compared to Experimental Results

complex	ΔG_{exp} (kJ/mol)	ΔG_{calc} (kJ/mol)			
		model 1 ^a	model 2 ^b	model 3 ^c	model 4 ^d
AuroraA-6BIO	-35.67	-31.80	-32.17	-30.83	-28.05
AuroraA-7BIO	-22.93	-27.52	-28.75	-25.47	-20.35
AuroraA-7BIMe	-18.92			-18.68	-18.40
AuroraA-7BIAC	-18.92			-15.42	-25.14
AuroraA-7FIO	-32.67	-24.82	-26.32	-30.79	-28.19
AuroraA-7CLIO	-18.92	-25.42	-26.07	-27.09	-23.50
AuroraA-7IIO	-18.93			-22.80	
AuroraA-7IIMe	-18.93			-25.55	
AuroraA-7IIAC	-18.93			-28.45	
AuroraB-6BIO	-34.66	-34.09	-35.87	-31.85	-32.22
AuroraB-7BIO	-30.60	-30.39	-33.98	-31.00	-31.15
AuroraB-7BIMe	-18.92			-23.20	-23.09
AuroraB-7BIAC	-26.94			-26.58	-28.06
AuroraB-7FIO	-29.55	-28.96	-28.96	-32.36	-32.00
AuroraB-7CLIO	-29.22	-31.79	-31.33	-33.76	-33.69
AuroraB-7IIO	-28.67			-30.98	
AuroraB-7IIMe	-18.93			-27.87	
AuroraB-7IIAC	-18.93			-27.86	
AuroraC-6BIO	-38.40	-36.10	-36.52	-32.06	-32.18
AuroraC-7BIO	-35.28	-36.99	-36.34	-34.34	-35.05
AuroraC-7BIMe	-28.66			-26.12	-25.64
AuroraC-7BIAC	-30.76			-32.11	-34.78
AuroraC-7FIO	-34.40	-32.72	-28.84	-32.99	-32.82
AuroraC-7CLIO	-34.66	-36.43	-31.86	-35.51	-35.87
AuroraC-7IIO	-35.67			-30.51	
AuroraC-7IIMe	-18.93			-27.27	
AuroraC-7IIAC	-26.10			-28.08	

^a In model 1, only unsubstituted oximes **4**, **5**, **9**, and **13** and water molecules A_w and B_w were considered, and arginines Arg137^{AurA}, Arg220^{AurA}, Arg81^{AurB}, and Arg47^{AurC} were constrained. ^b Same as model 1 but arginines were unconstrained. ^c Same as model 1, with the addition of substituted oximes **6** and **7** and water molecules C_w and D_w. ^d Same as model 3, with exclusion of water B_w.

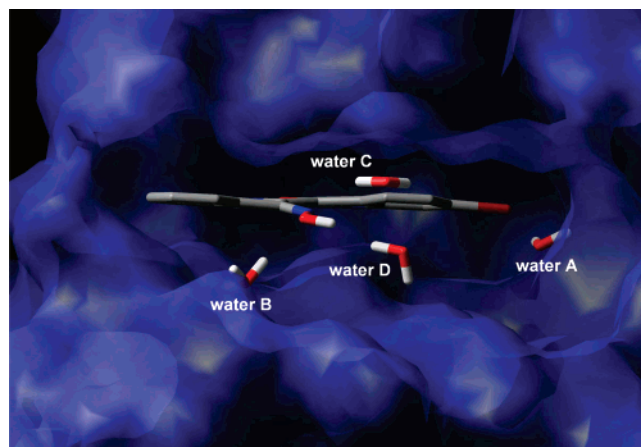


Figure 4. Four water molecules A_w, B_w, C_w, and D_w used in calculations in a depiction of 6BIO bound to Aurora A binding pocket. The receptor is represented by its the solvent-accessible surface.

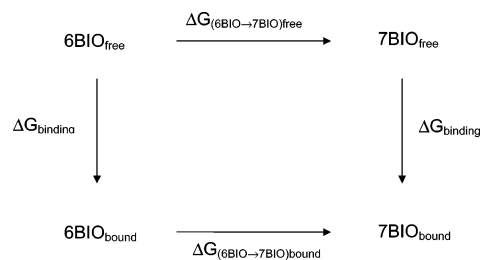
Interaction energies were first calculated for compounds 6BIO, 7BIO, 7FIO, and 7CLIO docked in each of the three Aurora kinases. A set of 12 points for a regression with two independent variables is statistically acceptable. Ligands having a substituted oxime were excluded from this set.

This primary model yielded a correlation with an r^2 of 0.54 (Table 2, model 1) and coefficients $\alpha = 0.26$, $\beta = 1.03$, and $\gamma = 151.0$. In all minimized complexes of Aurora A, water B_w participated, exhibiting stabilizing interactions. It received a hydrogen bond from the threonine hydroxyl and donated one to the oxime oxygen. In the Aurora B and C complexes, the critical glutamate was directly interacting with the oxime through a hydrogen bond.

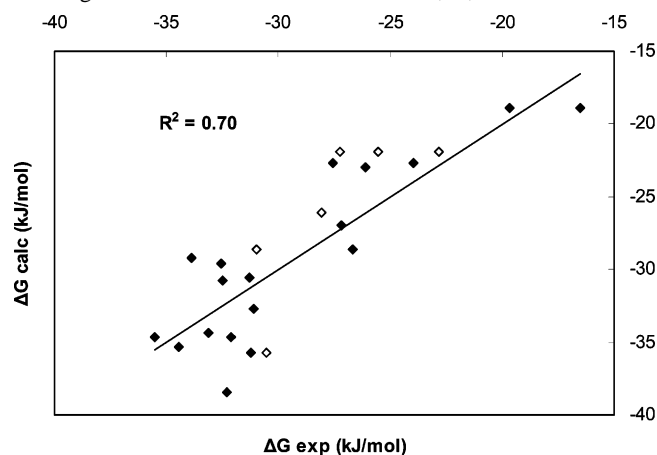
The next step of the model optimization was to test the influence of the two sets of constraints of the model. Removing the constraints applied on the three residues participating to the key hydrogen-bond pattern caused a small decrease of the correlation quality ($r^2 = 0.52$). A more significant decrease was caused by the subsequent removal of the arginine constraints, with r^2 reaching 0.43 (Table 2, model 2). In the resulting structures, the guanidine moiety of arginine was strongly attracted by the planar aromatic system of indirubin interacting intensively with it. The individual interaction energy terms were seriously influenced by the arginine mobility. All values were more negative and the new coefficients obtained ($\alpha = 0.13$, $\beta = 0.70$, and $\gamma = 99.5$) showed that the arginine side chain offered mainly hydrophobic interactions (coefficient β). The need for the arginine constraint could be interpreted either by the existence of a physical constraint on this residue, possibly an indirect interaction through water molecules with another residue located at some distance, or by a deficiency of the force field parametrization for the guanidine system.

In our stepwise construction and optimization of the model, the following step was to include oxime-substituted indirubins in the set of studied ligands. Biological results implied that these derivatives, and especially the methoximes, demonstrated a noteworthy decrease in binding affinity. The interpretation of these results would further validate our model. Including 7BIME and 7BIAC in the set of four ligands yielded a set of six ligands and a number of 18 points for a regression with two variables. The correlation obtained by this extended set of ligands with the docking parameters of the primary model yielded a very poor r^2 (0.39). The primary model obviously could not explain the reduced affinity of these analogues. From a structural point of view, the cause of the wrong estimation should be attributed to the interaction mode of the only part of the molecule that was altered, the substitution at position 3'. Upon docking, the methyl and acetyl groups of 7BIME and 7BIAC were located at the pocket entrance projecting toward the solvent. These nonpolar groups could not form any repulsive interactions or bad contacts with the receptor which would decrease the calculated binding affinity. On the contrary, the van der Waals interaction energy term was more negative, demonstrating the good hydrophobic interactions of the methyl and acetyl moieties with the aliphatic carbons of residues located on the glycine loop, the ribose site, and in the pocket entrance. Addition, in the scoring function, of a hydrogen-bond donor indicator describing the oxime substitution would be applicable. However, it was not considered as an elegant approach since it would reduce the molecular mechanics energy-derived scoring function to a semi-QSAR one. To address this problem in a way relevant to our MM approach, it was decided to model an energetic penalty by addition to the model of explicit water molecules. These molecules would be located at the entrance of the pocket where the methoxime and the acetoxime moieties of the docked inhibitors reside. The concept was to act as spatial antagonists of the methyl and acetyl substituents of the oxime. In order to do so, they would have to be constrained in place by a harmonic force. This manipulation was in modest analogy with the primary hydration shell method as it has been implemented in the study of the hydration of macromolecules.⁴⁰ In our case, two additional water molecules were included in the primary model, molecules C_w and D_w (Figure 4). Crystallographic water C_w (PDB atom 3055) is placed 2.8 Å from the backbone NH of Lys141, interacting with it through a hydrogen bond. Water D_w was not a part of the crystal structure but was hypothesized and positioned in the place occupied by the 3'-hydroxyl of the

Scheme 2. Thermodynamic Cycle Used for the Free Energy Perturbation Calculations



Scheme 3. Experimental versus Calculated Free Energies of Binding of Indirubins to Aurora Kinases A, B, and C^a



^a ΔG_{calc} is obtained from model 3 calculations. The derived scoring function is $\Delta G_{\text{calc}} = 0.27E_{\text{electrostatic}} + 0.63E_{\text{vanderWaal}} + 89.83$. The correlation coefficient r^2 is 0.70 and the standard error of estimate is 3.04 kJ/mol. (◆) Compounds used to construct the model (4, 5, 6, 7, 9, and 13); (◇) compounds that were predicted by the model (17, 18, and 19).

ADP-ribose of the structure. It is not unusual for water molecules bound in the ATP-binding pocket of kinases to be displaced by polar groups of the ligand that form similar electrostatic interactions, like in the case of CDK2. In that structure, two active-site waters of the apo structure are substituting for the adenine ring of ATP as it appears in the binary structure, forming similar hydrogen bonding interactions with the protein.⁴¹ Waters C_w and D_w were anchored by force constraints at the entrance of the ATP-binding pocket. Due to their reduced mobility, these two molecules would not be capable of performing large rotational or translational movements in the course of docking calculations, so their position and orientation was preoptimized.

The correlation obtained for the new model yielded the best r^2 (0.70) (Table 2, model 3; Scheme 3) and coefficients $\alpha = 0.27$, $\beta = 0.63$, and $\gamma = 89.8$. The interaction energy of the methoxime and acetoxime analogues was efficiently decreased by the steric repulsion with the two restrained waters. It seems reasonable that there is a physical meaning dictating the restriction of the mobility of water molecules located at the pocket entrance, and the need to restrain them could possibly be considered as more than technical. A possible explanation could be based on the equilibrium between enthalpic and entropic contributions of water molecules of the receptor hydration shell and especially at the ATP-binding pocket, in the energetics of ligand binding. Treating in such a way the defect of the primary model could be applicable in docking studies of other kinase-inhibitor complexes as well. In many series of kinase inhibitor analogues the molecule alterations are located at the side that is directed toward the pocket entrance-solvent interface. The effect of these alterations on binding affinity cannot always be modeled successfully by any direct

interaction with the receptor. Water molecules constrained at the entrance could offer not only unfavorable repulsive but also favorable electrostatic or hydrogen-bonding interactions, provided that they have full rotational and controlled translational freedom.

The last trial in order to optimize the model was the exclusion of water B_w . The model yielded a correlation with $r^2 = 0.64$ (Table 2, model 4) and coefficients $\alpha = 0.30$, $\beta = 0.78$, and $\gamma = 116.3$. This was a fair indication of the functionality of water B_w in the studied system.

Model 3 thus represents the best model obtained by docking–scoring calculations. The predictability of the model was examined by the calculation of the ΔG of binding of the 7-iodo substituted compounds **17**, **18**, and **19** which were not used in the model construction. Each compound was docked in the binding pocket of each of the three kinases by superposition with the reference ligand used in model construction. Then it was subjected to an interaction energy calculation on the basis of the scoring function obtained by model 3. The calculated $\Delta G_{\text{binding}}$ values (Table 2) showed good agreement with experimental data as presented in Scheme 3, with rms deviation of prediction at 6.19 kJ/mol (1.48 kcal/mol), accuracy typical for this kind of calculations.^{42–44} It is interesting to note that the predicting ability of the model is also apparent in the case of the 7-fluoro-substituted oxime **13**. This compound does not demonstrate the selectivity profile demonstrated by the 7-chloro, 7-bromo, and 7-iodo analogues but inhibits with equally high potency all Aurora kinases as well as the CDKs and GSK-3 β .¹⁶ The $\Delta G_{\text{binding}}$ of compound **13** is correctly predicted by the model within 2.11 kJ/mol (0.51 kcal/mol) for each of the three Aurora kinases. It should be noted that the differences observed in the biological activity of 7-substituted oximes between Aurora B and C cannot be explained by this model, as these kinases exhibit identical active-site topology as resulting from homology modeling. Given that differences in $\Delta G_{\text{binding}}$ among indirubin analogues within the same kinase follow the same trend, these biological results could be interpreted as variations in the degree of activation of each kinase in the assay. Moreover, the activation of the enzyme could also control conformational equilibrium of flexible structural elements like the glycine and activation loops. The conformation of these regulatory parts of the receptor influences access of the inhibitor in the active site; however, such structural variations cannot be simulated by homology modeling methods.

Molecular Dynamics and Free Energy Perturbation. The docking approach shed much light on the energetic background of the selectivity phenomenon as well as on several methodological aspects. However, it was considered that utilizing alternative molecular-mechanics based methods to cross-validate our semiempirical results would be meaningful. We decided to study 6BIO and 7BIO binding by two additional approaches, Molecular Dynamics and Free Energy Perturbation.

Molecular dynamics (MD) runs of 200 ps were performed on the minimized complexes of 6BIO and 7BIO bound in Aurora A and B. In the evolution of the simulation, the hydrogen-bond donor/acceptor distances and angles were monitored and the results are summarized in Supporting Information (Table S3). The deformation of the third bond is clearly reflected in the average distance monitored throughout the run between the proton of the lactam nitrogen of indirubin and the receptor. The average distance is 2.5 Å in the case of 6BIO–Aurora A but it is raised to 3.8 Å in the 7BIO–Aurora A complex. At 3.8 Å the bond is practically nonexistent. The bond deformation

Table 3. Relative Free Energy $\Delta\Delta G$ for the Mutation of 6BIO to 7BIO Bound to Aurora A and B from Free Energy Perturbation Calculations, Compared to Experimental Results^a

receptor/mutation	$\Delta\Delta G_{\text{exp}}$ (kJ/mol)	$\Delta\Delta G_{\text{calc}}$ (kJ/mol)	
		min substr	ext substr
Aurora A/6BIO \rightarrow 7BIO	+12.63	+18.41	+6.61
Aurora B/6BIO \rightarrow 7BIO	+4.03	+6.78	+1.32

^a Min substr concerns calculations performed with the minimal substructure, where all protein atoms were considered as rigid and ligand atoms were free to move. In extended substructure (ext substr), all ligand atoms and atoms belonging to a sphere of 3 Å around the ligand were free to move.

also occurs in the case of Aurora B, where the distance is raised from 2.8 Å (6BIO) to 3.7 Å (7BIO). At the same time the stabilizing interaction between the ligand and the critical glutamate of Aurora B is not only sustained but gains in strength as the oxime hydrogen of 7BIO approaches the carboxylate oxygen of glutamate, moving 0.4 Å closer, and the hydrogen-acceptor angle is optimized by 20°. An additional observation was derived from MD runs concerning the attitude of the individual water molecules included in our model. In the evolution of MD, water molecules C_w and D_w (unconstrained in MD runs) were completely displaced from starting coordinates. On the contrary, the water mediating the interaction between threonine217 of Aurora A and the ligand oxime (water B_w), as well as the buried water A_w , demonstrated very good stability. This could be an additional indication of the important role the two latter molecules play in the complexation events. While waters C_w and D_w simulate the penalty of the entropic or other energy terms on binding, waters A_w and B_w can be considered as functional.

The implementation of free energy perturbation (FEP) is believed to be the most accurate method to validate our hypothesis.⁴⁵ It is a first principles method that can calculate with high precision the relative free energy of binding of two structurally related ligands, however computationally demanding. The conversion of 6BIO to 7BIO is within the method limits. A fast FEP protocol was used, where several approximations were held. The explicit solvent was replaced by the implicit GB/SA model,⁴⁶ and apart from the ligand atoms, all other atoms of the system were kept frozen. System A (6BIO bound to the protein) was mutated to system B (7BIO bound to the protein). This mutation evolved in 50 windows. For each window, ensemble averages were collected for various energy terms by MD simulations of 500 ps. The thermodynamic cycle used to determine the relative free energy of binding is presented in Scheme 2. $\Delta\Delta G_{\text{binding}}$ was calculated as

$$\Delta\Delta G_{\text{binding}}(6\text{BIO} \rightarrow 7\text{BIO}) = \Delta G_{(6\text{BIO} \rightarrow 7\text{BIO})\text{bound}} - \Delta G_{(6\text{BIO} \rightarrow 7\text{BIO})\text{free}} \quad (2)$$

The calculated difference in free energy of binding of 6BIO and 7BIO was in good agreement with experimental results (Table 3) with the largest error being +5.78 kJ/mol (+1.38 kcal/mol). This agreement is typical for FEP simulations.⁴⁵ An inspection of the intermediate structures' trajectories of the mutation provided us with two interesting pieces of information. The ligand was gradually changing its orientation in the active site, and the distance between the ligand lactam nitrogen and the kinase backbone (third hydrogen bond) was gradually increasing (Figure 5). In the Aurora A structure, the distance was increased from 2.8 to 3.6 Å, and in Aurora B, from 3 to 3.7 Å. The distance of the second hydrogen bond between the inhibitor lactam carbonyl and the receptor backbone was also

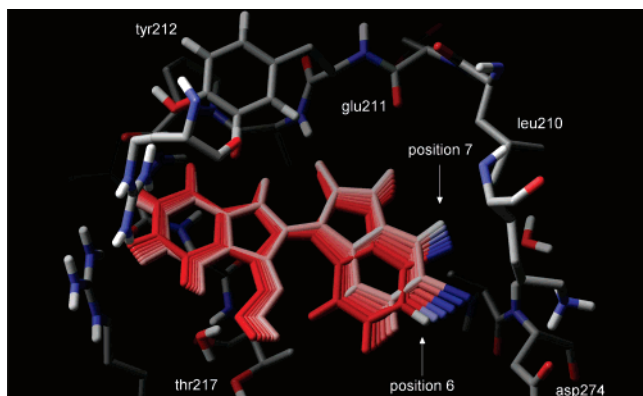


Figure 5. Conversion of the bromine atom at position 6 to hydrogen (blue turning to white) and the reverse conversion at position 7 performed in the free energy perturbation calculation of the relative free energy of binding between 6BIO (white) and 7BIO (red) in Aurora A. The mutation of the hydrogen atom at position 7 to bromine induces a steric clash that reorients 7BIO in the pocket. As a result, the third hydrogen bond between the lactam hydrogen of indirubin and the backbone carbonyl of Glu211 is distorted. This accounts for the loss of affinity demonstrated by 7BIO for Aurora A.

increased but only slightly. These observations were in very good agreement with the above-mentioned MD simulations. The same pattern of bond deformation was observed. They were also in accordance with our selectivity hypothesis, as they support the concept that the cause of the selectivity profile of 7BIO is exclusively located in the different orientations that 6BIO and 7BIO adopt in the ATP-binding pocket and the impact of this orientation on the strength of the hydrogen bonds formed between each ligand and its kinase receptor. An additional set of FEP calculations was performed where all atoms within 3 Å from the ligand were free to move. This set was intended to monitor the influence of the freezing atom approximation to the results. The results of both calculations are summarized in Table 3. This second set with the extended moving atom substructure yielded also a good correlation with the experimental free energies of binding. In this case, the calculated free energies of binding changed to more negative values with the largest error at -6.01 kJ/mol. However, the relative difference between the $\Delta\Delta G$ of binding tended to be conserved between the two calculations. The performance of the fast FEP protocol was encouraging since it was designed with the purpose of combining efficiently speed and computational precision. We are currently working on optimizing the fast FEP protocol as a high-precision method for studying the phenomenon of selectivity among kinase inhibitors where small differences in structure induce major differences in potency.

Conclusions

The evolutionary conservation of the kinase active-site topology is dictated by the special character of the biochemical processes occurring there: the binding of ATP, the loosening of the covalently bound terminal phosphate group, and its final transfer to the substrate. Differences among kinase active sites are usually constituted of variations of a very small number of residues. However, these seemingly minor variations are the factors that exclusively determine the selectivity demonstrated by several classes of inhibitors. The interplay between structure and function in the binding process of small molecules acting as inhibitors is of great interest.

Our study presents an integrated attempt to explain and verify through computational methods the fact that 7BIO selectively inhibits Aurora kinases B and C, discriminating them from their

homologous Aurora A, while 6BIO demonstrates no selectivity and binds equally well to the three Aurora homologues. The selectivity hypothesis can be accounted for by a single active-site residue difference revealed by the sequence alignment. This critical residue is a threonine in Aurora A while it is a glutamate in Aurora B and C. Homology models were built for Aurora B and C, and docking experiments followed by interaction energy calculations shed light on docking events and validated this hypothesis. When the indirubin substitution turns from a 6-bromo to a 7-bromo, a repositioning of the ligand then occurs in the pocket and a partial deformation of the key hydrogen bonds involved in binding is observed. This perturbation however, is efficiently counterbalanced by a novel favorable interaction provided by the critical glutamate only in the Aurora B and C kinases. The construction of a model correlating experimental and calculated binding affinities not only verified the aforementioned hypothesis but also provided valuable information with respect to methodology. In order to simulate binding events in a reproducible way and without neglecting the static but indisputably correct depiction of binding provided by crystallography, we had to address important methodological issues. Our results show the following: (a) The energetic well where the key hydrogen bonds of the complex are formed can be adequately used as a reference state of the bound ligand. The energy minimum could be determined by the application of selected constraints on the residues participating in HB formation and subsequently relaxed by unconstrained energy minimization. (b) When a side of the ATP-binding pocket is defined by an arginine side chain, as in many kinases, then a restriction of its mobility is necessary for obtaining a reliable interaction energy calculation. (c) Identical topology of critical residues is a requirement for the construction of a scoring function correlating data from different but homologous kinase targets. (d) Inclusion in calculations of the water molecule mediating interactions between the oxime group of indirubin and the kinase is encouraged since it improves model quality. (e) There is a need to model a steric penalty for ligands carrying bulky and apolar chemical groups that are oriented toward the ATP-binding pocket entrance upon binding. This need arises from the observed decrease of their potency. Their reduced affinity is not reproducible in structural models by any steric repulsions. In this study the penalty consists of constrained water molecules occupying the pocket entrance.

Furthermore, the hypothesis was validated by molecular dynamics simulations, where all bond deformations and formations that were described by static docking calculations were observed. Finally, by implementing a fast free energy perturbation protocol, we have calculated with precision the relative binding energies, which are within the typical limits of the method. FEP also demonstrated in the most precise way that the cause of selectivity is the aforementioned bond deformations and subsequent formations and that similar events can be fairly approached by our fast protocol. It is hoped that such a study would assist in bridging the gap between bioinformatics and theory on one hand and biological responses and experiments on the other hand. It would also be a good indication of the important role computational methods can play in the drug discovery process.

Experimental Section

Molecular Modeling. The sequences of Aurora B and C were downloaded from Swiss-Prot server (primary accession numbers: Aur.B Q96GD4, Aur.C Q9UQB9) and were aligned with the sequence of Aurora A (O14965) by use of Clustalw v.1.82 with default settings and the alignment depiction by ESPript.^{35,47}

Homology modeling was performed by MODELLER v.6 with the utilization of the *do_loop* routine for loop modeling and a refinement level set by the *do_refinement_3* command. For the stochastic dynamics simulation of the homology models, the all-atom AMBER94 force field was used. All bond lengths were constrained by the SHAKE algorithm, and simulations were carried out with a 1 fs time step at 300 K. Adjustments prior to docking calculations were performed in the side-chain χ_n torsions of residues Glu161^{AurB}, Glu127^{AurC}, Lys164^{AurB}, and Lys130^{AurC}. After homology modeling refinement, these residues did not have exactly the same rotamer conformation in Aurora B and C. The side chain of glutamate was oriented toward the ATP-binding pocket entrance in order to allow an interaction with the oxime hydroxyl of the ligands, while the lysine side chain was oriented so that the quaternary ammonium group would point to the bulk solvent, as it was observed in the crystal structure of homologous kinases bearing a corresponding lysine residue like the *Xenopus laevis* Aurora B (2BFY). Docking was performed with the AMBER* force field, and the EMBRACE routine was used for interaction energy calculations. Force constraints were applied by the "Freeze" option of Macromodel for the restrained residues and by 500 kJ harmonic constraints for waters C_w and D_w. The positions of these two molecules were preoptimized prior to interaction energy calculations. They were reoriented manually in order to form a net of hydrogen-bonding interactions with each other and with two selected residues of the pocket entrance, a lysine backbone NH at the glycine loop (Lys141^{AurA}, Lys85^{AurB}, Lys51^{AurC}), and a glutamate backbone carbonyl at the ribose site (Glu260^{AurA}, Glu204^{AurB}, Glu170^{AurC}). Then a minimization followed with distance constraints overlapping with the bonds, which resulted in a network of three hydrogen bonds connecting the glycine loop with the pocket threshold through waters C_w and D_w. All SD, MD, and docking simulations were performed with Macromodel v.9 package.⁴⁸ In the FEP simulation, the mutation was based on Zwanzig's equation and the single topology method as implemented in Macromodel v.5.⁴⁹ FEP simulations were carried out with the AMBER* force field, a time step of 0.5 fs, and 50 MD runs of 500 ps, each one preceded by 100 ps equilibration. In each window all atomic parameters involved in calculations were generated by a mixing of the starting and ending parameters. The parameters concerning the atoms in positions 6 (bromine turning to a hydrogen) and 7 (hydrogen turning to a bromine) of indirubin were scaled by

$$\text{parameter} = \lambda(\text{starting value}) + (1 - \lambda)(\text{ending value}) \quad (3)$$

where lambda (λ) describes the percentage of the mutation and is 0 for the starting state and 1 for the final. The Truncated Newton conjugate gradient minimizer and the GB/SA implicit solvent model were used in all simulations. All ligand partial charges were calculated in a semiempirical level by MOPAC6 using the AM1 Hamiltonian and the eigenvector Following minimizer (keywords used NOMM AM1 EF).⁵⁰ The experimental free energies of binding were approximated from the IC₅₀ values by use of eq 4, with RT equal to 2.49 kJ/mol and IC₅₀ values in moles per liter:

$$\Delta G_{\text{exp}} \approx RT \ln IC_{50} \quad (4)$$

A value of 500 μM was attributed to inactive compounds used for the model building, demonstrating IC₅₀ over 100 μM .

Protein Kinase Assays: (A) Biochemical Reagents. Sodium ortho-vanadate, EDTA, Mops, β -glycerophosphate, phenylphosphate, dithiothreitol (DTT), glutathione-agarose, glutathione, bovine serum albumin (BSA), nitrophenylphosphate, and myelin basic protein were obtained from Sigma Chemicals. [γ -³³P]ATP was obtained from Amersham.

(B) Kinase Assays. Recombinant human Aurora A, B, and C (a generous gift from M. Kubbutat, ProQinase) assays were carried out at 30 °C for 30 min by use of 15 μM [γ -³³P]ATP (3000 Ci/mmol, 1 mCi/mL) in buffer C [60 mM β -glycerophosphate, 15 mM p-nitrophenylphosphate, 25 mM Mops (pH 7.2), 5 mM EGTA, 15 mM MgCl₂, 1 mM DTT, 1 mM sodium vanadate, and 1 mM

phenylphosphate], with myelin basic protein (1 mg/mL) as a substrate in a final volume of 30 μL . The reactions were stopped by spotting 25 μL onto p81 phosphocellulose papers (Whatman), which were washed 5 times in 1% phosphoric acid. Scintillation fluid was added and the radioactivity was measured in a scintillation counter. To determine the IC₅₀ values, blank values were subtracted and activities expressed in percent of the maximal activity, that is, in the absence of kinase inhibitors.

Acknowledgment. This research was supported by the General Secretariat of Research and Technology of Greece, PENED program (V.M.), University of Athens program Kapodistrias, and grants from the EEC (FP6-2002-Life Sciences & Health, Pro-Kinase Research Project) (L.M.) and the Cancero-pole Grand-Ouest (L.M.).

Supporting Information Available: Electrostatic and van der Waals calculated energy terms used for the calculation of free energy of binding (Table S1), weighting coefficients α , β , and γ used in the equation for the calculation of free energy of binding (Table S2), and averages from the 200 ps MD simulations for 6BIO and 7BIO complexed with Aurora A and B (Table S3). This material is available free of charge via the Internet at <http://pubs.acs.org>.

References

- (1) Cohen, P. Protein kinases—the major drug targets of the twenty-first century? *Nat. Rev. Drug Discovery* **2002**, *1*, 309–315.
- (2) Dancey, J.; Sausville, E. A. Issues and progress with protein kinase inhibitors for cancer treatment. *Nat. Rev. Drug Discovery* **2003**, *4*, 296–313.
- (3) Hirota, S.; Isozaki, K.; Moriyama, Y.; Taniguchi, M.; Nakamura, J.; Okazaki, T.; Kitamura, Y. Gain-of-function mutations of c-kit in human gastrointestinal stromal tumors. *Science* **1998**, *279*, 577–580.
- (4) Blume-Jensen, P.; Hunter, T. Oncogenic kinase signaling. *Nature* **2001**, *411*, 355–365.
- (5) Marshall, J. C. Ras effectors. *Curr. Opin. Cell Biol.* **1996**, *8*, 197–204.
- (6) Sherr, C. J. The Pezcoller lecture: Cancer cell cycles revisited. *Cancer Res.* **2000**, *60*, 3689–3695.
- (7) Sausville, E.; Johnson, J.; Alley, M.; Zaharevitz, D.; Senderowich, A. M. Inhibition of CDKs as a therapeutic modality. *Ann. N.Y. Acad. Sci.* **2000**, *910*, 207–222.
- (8) Yarden, Y.; Sliwkowski, M. X. Untangling the ErbB signaling network. *Nat. Rev. Mol. Cell Biol.* **2001**, *2*, 127–137.
- (9) Druker, B. J.; Talpaz, M.; Resta, D. J.; Peng, B.; Buchdunger, E.; Ford, J. M.; Lydon, N. B.; Kantariian, H.; Capedeville, R.; Ohno-Jones, S.; Sawyer, C. L. Efficacy and safety of a specific inhibitor of Bcr-Abl tyrosine kinase in chronic myeloid leukemia. *N. Engl. J. Med.* **2001**, *344*, 1031–1037.
- (10) Vieth, M.; Sutherland, J. J.; Robertson, D. H.; Campbell, R. M. Kinomics: characterizing the therapeutically validated kinase space. *Drug Discovery Today* **2005**, *10*, 839–846.
- (11) Hoessel, R.; Leclerc, S.; Endicott, J.; Noble, M.; Lawrie, A.; Tunnah, P.; Leost, M.; Damiens, E.; Marie, D.; Marko, D.; Niederberger, E.; Tang, W.; Eisenbrand, G.; Meijer, L. The active constituent of a Chinese antileukaemia medicine inhibits cyclin-dependent kinases. *Nat. Cell Biol.* **1999**, *1*, 60–67.
- (12) Davies, T. G.; Tunnah, P.; Meijer, L.; Marko, D.; Eisenbrand, G.; Endicott, J. A.; Noble, M. E. M. Inhibitor binding to active and inactive CDK2. The crystal structure of a CDK2-cyclin A/indirubin-5-sulphonate. *Structure* **2001**, *9*, 389–397.
- (13) Meijer, L.; Skaltsounis, A. L.; Magiatis, P.; Polychronopoulos, P.; Knockaert, M.; Leost, M.; Ryan, X. P.; Vonica, C. A.; Brivanlou, A.; Dajani, R.; Crovace, C.; Tarricone, C.; Musacchio, A.; Roe, S. M.; Pearl, L.; Greengard, P. GSK-3-selective inhibitors derived from Tyrian purple indirubins. *Chem. Biol.* **2003**, *10*, 1255–66.
- (14) Polychronopoulos, P.; Magiatis, P.; Skaltsounis, A. L.; Myrianthopoulos, V.; Mikros, E.; Tarricone, A.; Musacchio, A.; Roe, M.; Pearl, L.; Leost, M.; Greengard, P.; Meijer, L. Structural basis for the synthesis of indirubins as potent and selective inhibitors of glycogen synthase kinase-3 and cyclin-dependent kinases. *J. Med. Chem.* **2004**, *47*, 935–946.
- (15) Ferandin, Y.; Bettayeb, K.; Kritsanida, M.; Lozach, O.; Polychronopoulos, P.; Magiatis, P.; Skaltsounis, A.-L.; Meijer, L. 3'-Substituted 7-halogenoindirubins, a new class of cell death inducing agents. *J. Med. Chem.* **2006**, *49*, 4638–4649.

- (16) Ribas, J.; Bettayeb, K.; Ferandin, Y.; Knockaert, M.; Garrofé-Ochoa, X.; Totzke, F.; Schächtele, C.; Mester, J.; Polychronopoulos, P.; Magiatis, P.; Skaltsounis, A.-L.; Boix, J.; Meijer, L. 7-Bromoindirubin-3'-oxime induces caspase-independent cell death. *Oncogene* **2006**, *25*, 6304–6318.
- (17) Bolanos-Garcia, V. Aurora kinases. *Int. J. Biochem. Cell Biol.* **2005**, *37*, 1572–1577.
- (18) Carmena, M.; Earnshaw, W. C. The cellular geography of aurora kinases. *Nat. Rev. Mol. Cell Biol.* **2003**, *4*, 842–854.
- (19) Giet, R.; Petrelli, C.; Prigent, C. Aurora kinases, aneuploidy and cancer, a coincidence or a real link? *Trends Cell Biol.* **2005**, *15*, 241–250.
- (20) Ducat, D.; Zheng, Y. Aurora kinases in spindle assembly and chromosome segregation. *Exp. Cell Res.* **2004**, *301*, 60–67.
- (21) Katayama, H.; Brinkley, W.; Sen, S. The Aurora kinases: Role in cell transformation and tumorigenesis. *Cancer Metastasis Rev.* **2003**, *22*, 451–464.
- (22) Bischoff, J. R.; Anderson, L.; Zhu, Y.; Mossie, K.; Ng, L.; Sousa, B.; Schryver, B.; Flanagan, P.; Clairvoyant, F.; Ginther, C.; Chan, C. S.; Novotny, M.; Slamon, D. J.; Plowman, G. D. A homologue of *Drosophila* aurora kinase is oncogenic and amplified in human colorectal cancers. *EMBO J.* **1998**, *17*, 3052–3065.
- (23) Tanaka, T.; Kimura, M.; Matsunaga, K.; Fukada, D.; Mori, H.; Okano, Y. Centrosomal kinase AIK1 is overexpressed in invasive ductal carcinoma of the breast. *Cancer Res.* **1999**, *59*, 2041–2044.
- (24) Han, H.; Bearss, D.; Browne, L. W.; Calaluce, R.; Nagle, R. B.; Von Hoff, D. Identification of differentially expressed genes in pancreatic cancer cells using cDNA microarray. *Cancer Res.* **2002**, *62*, 2890–2896.
- (25) Sen, S.; Zhou, H.; Zhang, R. D.; Yoon, D. S.; Vakar-Lopez, F.; Ito, S.; Jiang, F.; Johnston, D.; Grossman, H. B.; Ruirok, A. C.; Katz, R. L.; Brinkley, W.; Czerniak, B. Amplification/overexpression of a mitotic kinase gene in human bladder cancer. *J. Natl. Cancer Inst.* **2002**, *94*, 1320–1329.
- (26) Katayama, H.; Sasai, K.; Kawai, H.; Yuan, Z.; Bondaruk, J.; Suzuki, F.; et al. Phosphorylation by aurora kinase A induces Mdm2-mediated destabilization and inhibition of p53. *Nat. Genet.* **2004**, *36*, 55–62.
- (27) Adams, R. R.; Eckley, D. M.; Vagnarelli, P.; Wheatley, S. P.; Gerloff, D. L.; Mackay, A. M.; Svingen, P. A.; Kaufmann, S. H.; Earnshaw, W. C. Human INCENP colocalizes with the Aurora-B/AIRK2 kinase on chromosomes and is overexpressed in tumour cells. *Chromosoma* **2001**, *110*, 65–74.
- (28) Ota, T.; Suto, S.; Katayama, H.; Han, Z. B.; Suzuki, F.; Maeda, M.; Tanino, M.; Terada, Y.; Tatsuka, M. Increased mitotic phosphorylation of histone H3 attributable to AIM-1/Aurora-B overexpression contributes to chromosome number instability. *Cancer Res.* **2002**, *62*, 5168–5177.
- (29) Hauf, S.; Cole, R. W.; LaTerra, S.; Zimmer, C.; Schnapp, G.; Walter, R.; Heckel, A.; van Meel, J.; Rieder, C. L.; Peters, J. M. The small molecule Hesperadin reveals a role for Aurora B in correcting kinetochore–microtubule attachment and in maintaining the spindle assembly checkpoint. *J. Cell Biol.* **2003**, *161*, 281–294.
- (30) Harrington, E. A.; Bebbington, D.; Moore, J.; Rasmussen, R. K.; Ajose-Adeogun, A. O.; Nakayama, T.; Graham, J. A.; Demur, C.; Hercend, T.; Diu-Hercend, A.; Su, M.; Golec, J. M.; Miller, K. M. VX-680, a potent and selective small-molecule inhibitor of the Aurora kinases, suppressed tumor growth in vivo. *Nat. Med.* **2004**, *10*, 262–267.
- (31) Cheetham, G.; Knegt, R. M.; Coll, J. T.; Rewick, S. B.; Swenson, L.; Weber, P.; Lippke, J. A.; Austen, D. A. Crystal structure of Aurora-2, an oncogenic serine/threonine kinase. *J. Biol. Chem.* **2002**, *277*, 42419–42422.
- (32) Nowakowski, J.; Cronin, C. N.; McRee, D. E.; Knuth, M. W.; Nelson, C. G.; Pavletich, N. P.; Rogers, J.; Sang, B. C.; Scheibe, D. N.; Swanson, R. V.; Thomson, D. A. Structures of the cancer-related aurora-A, FAK, and EphA2 protein kinases from nanovolume crystallography. *Structure* **2002**, *10*, 1659–1667.
- (33) Sali, A.; Potterton, L.; Yuan, F.; van Vlijmen, H.; Karplus, M. Evaluation of comparative protein modeling by MODELLER. *Proteins: Struct., Funct., Genet.* **1995**, *23*, 318–326.
- (34) Laskowski R., MacArthur M., Moss D., Thornton J. PROCHECK: A program to check the stereochemical quality of protein structures. *J. Appl. Crystallogr.* **1991**, *26*, 283–291.
- (35) <http://www.ch.embnet.org/software/ClustalW.html>.
- (36) Huang, D.; Cafilisch, A. Efficient evaluation of binding free energy using continuum electrostatics solvation. *J. Med. Chem.* **2004**, *47*, 5791–5797.
- (37) Cochran, S.; Li, C. P.; Bytheway, I. An experimental and molecular-modeling study of the binding of linked sulfated tetracyclitols to FGF-1 and FGF-2. *ChemBioChem* **2005**, *6*, 1882–1890.
- (38) Toung, B. A.; Reynolds, C. H. Calculation of the binding affinity of β -secretase inhibitors using the linear interaction energy method. *J. Med. Chem.* **2003**, *46*, 2074–2082.
- (39) Ferrara, P.; Curioni, A.; Vangrevelinghe, E.; Meyer, T.; Mordasini, T.; Andreoni, W.; Acklin, P.; Jacoby, E. New scoring functions for virtual screening from molecular dynamics simulations with a quantum-refined force-field (QRFF-MD). Application to cyclin-dependent kinase 2. *J. Chem. Inf. Model.* **2006**, *46*, 254–263.
- (40) Beglov, D.; Roux, B. Dominant solvation effects from the primary shell of hydration: Approximation for molecular dynamics simulations. *Biopolymers* **1995**, *35*, 171–178.
- (41) Schulze-Gahmen, U.; De Bondt, H.; Kim, S. H. High-resolution crystal structures of human cyclin-dependent kinase 2 with and without ATP: Bound waters and natural ligand as guides for inhibitor design. *J. Med. Chem.* **1996**, *39*, 4540–4546.
- (42) Barril, X.; Soliva, R. Molecular Modelling. *Mol. BioSyst.* **2006**, *2*, 660–681.
- (43) Pierce, A. C.; Jorgensen, W. L. Estimation of binding affinities for selective thrombin inhibitors via Monte Carlo simulations. *J. Med. Chem.* **2001**, *44*, 1043–1050.
- (44) Singh, P.; Mhaka, M. A.; Christensen, S. B.; Gray, J. J.; Denmeade, S. R.; Isaacs, J. T. Applying linear interaction energy method for rational design of noncompetitive allosteric inhibitors of the sarco- and endoplasmic reticulum calcium-ATPase. *J. Med. Chem.* **2005**, *48*, 3005–3014.
- (45) Kollman, P. Free energy calculations: Applications to chemical and biochemical phenomena. *Chem. Rev.* **1993**, *93*, 2395–2417.
- (46) Still, C. W.; Tempczyk, A.; Hawley, R. C.; Hendrickson, T. Semi-analytical treatment of solvation for molecular mechanics and dynamics. *J. Am. Chem. Soc.* **1990**, *112*, 6127–6129.
- (47) Gouet, P.; Courcelle, E.; Stuart, D. I.; Metz, F. ESPript: multiple sequence alignments in postscript format. *Bioinformatics* **1999**, *15*, 305–308.
- (48) Mohamadi, F.; Richards, N. G.; Guida, W. C.; Liskamp, R.; Lipton, M.; Caufield, C.; Chang, G.; Hendrickson, T.; Still, W. C. Macro-model-An integrated software system for modeling organic and bioorganic molecules using molecular mechanics. *J. Comput. Chem.* **1990**, *11*, 440–467.
- (49) Zwanzig, R. W. High temperature equation of state by a perturbation method. I. Nonpolar gases. *J. Chem. Phys.* **1954**, *22*, 1420–1426.
- (50) Stewart, J. J. P. MOPAC—A semiempirical molecular orbital program. *J. Comput.-Aided Mol. Des.* **1990**, *4*, 1–105.

JM070077Z